Application of a Simulation Platform for the Study and Experimental Comparison of PEM Electrolyzer Models

Antonio José Calderón[a], Francisco Javier Folgado[b], David Calderón[c] and Isaías González[d]
Department of Electrical Engineering, Electronics and Automation, Universidad de Extremadura, Avenida de Elvas, s/n, 06006, Badajoz, Spain

Keywords: PEM Electrolyzer, Hydrogen, Renewable Energies, Smart Microgrid, Simulation.

Abstract: In the last decades, hydrogen has been a trend in the energy sector as it has been employed as an energy carrier in applications based on Renewable Energy Sources (RES). In this context, RES-based smart grids and microgrids use devices called electrolyzers to generate hydrogen. The implementation of this device in a real installation faces difficulties due to its complex operation and the diversity of variables involved. Therefore, a prior study is essential to understand the behavior of these devices and to achieve correct implementation and management. This paper describes the application of a simulation platform for the study of Proton Exchange Membrane Electrolyzers (PEMEL), as well as the comparison of the data obtained through simulation and those reported from an experimental PEMEL operating within a RES-powered smart microgrid hybridized with green hydrogen. The principle of operation of the simulation platform is presented together with the models selected for this research. The experimental PEMEL is framed in the operation of the smart microgrid, where its automation equipment and the interaction between them are described. Furthermore, the process followed to obtain the simulated and experimental data is detailed. Finally, a case study is reported where simulated and experimental results are compared.

1 INTRODUCTION

Hydrogen is a gaseous element under ambient conditions, whose chemical properties give it high relevance in applications across various fields. In the field of chemical industry, hydrogen is present in petroleum refining processes (Manna et al., 2021), as well as in the production processes of ammonia (Ishaq et al., 2021; Manna et al., 2021) and urea (Ishaq et al., 2021). In recent decades, climate changes resulting from the use of fossil fuels, as well as the scarcity of these resources and the progressive increase in global energy demand have driven the research and development of new technologies for the utilization of new energy resources such as hydrogen. The energy characteristics of this element have made it a promising energy carrier (Abdin et al., 2020) to address these challenges, fostering the transformation of production processes to include hydrogen generation (Ishaq et al., 2022; Tang et al., 2023), storage (Tang et al., 2023), and utilization (Ishaq et al., 2022) within industries.

Currently, hydrogen has become a revolutionary trend in the energy sector, driving advancements in fields such as automotive (Aminudin et al., 2023), energy transportation (Niermann et al., 2019), as well as the reduction of fossil fuel consumption (Potashnikov et al., 2022) and the exploitation of Renewable Energy Sources (RES) (Sarker et al., 2023). In the context of RES-based applications, the current trend leans towards the integration of hydrogen in systems such as smart grids or microgrids. In these systems, hydrogen serves as a supportive element to stabilize short and medium-term energy fluctuations caused by the variability of RES (Atlam & Kolhe, 2011). In these applications, devices called electrolyzers are employed. Electrolyzers are hydrogen generation devices based on the electrolysis process. More specifically, in RES-based systems, the use of Proton Exchange

[a] https://orcid.org/0000-0003-2094-209X
[b] https://orcid.org/0000-0001-6010-0685
[c] https://orcid.org/0009-0004-6569-4581
[d] https://orcid.org/0000-0001-5645-3832

Calderón, A., Folgado, F., Calderón, D. and González, I.
Application of a Simulation Platform for the Study and Experimental Comparison of PEM Electrolyzer Models.
DOI: 10.5220/0012202800003543
In *Proceedings of the 20th International Conference on Informatics in Control, Automation and Robotics (ICINCO 2023) - Volume 2*, pages 289-296
ISBN: 978-989-758-670-5; ISSN: 2184-2809

Membrane Electrolyzers (PEMEL) is common due to their features that allow for a rapid response to variations in input setpoints (Feng et al., 2017).

The integration of PEMEL into systems like microgrids is not immediate due to their complex operation and the diversity of factors to consider for proper operation (Folgado et al., 2022). Therefore, it is necessary to conduct a preliminary study in order to understand the behavior and operation of these devices, as well as the key variables involved and their relationships. This knowledge is crucial for implementing PEMEL and ensuring safe long-term behavior and operation, thus preventing the occurrence of degradation mechanisms that reduce performance and equipment lifespan (Feng et al., 2017). To understand the operation of PEMEL, models are used that describe their electrochemical behavior and associate their mechanisms with interrelated variables. In (Falcão & Pinto, 2020), a set of models described by various authors is reviewed, examining the relationship between variables such as voltage, working temperature, working pressure, current density, and the effects resulting from their variations.

This paper describes the application of a simulation platform for the study and comparison of PEMEL models and an experimental PEMEL integrated into a prototype smart microgrid powered by RES and hybridized with green hydrogen. In this work, the operating principle of the simulator, the equipment comprising the smart microgrid, and their interconnection are described, as well as the process of acquiring simulated and experimental data. Finally, a case study is presented where the behavior of the models and the real device is compared under identical operating conditions.

This work is framed within a Research and Development (R&D) project focused on the employment of hydrogen and its exploitation as an energy carrier through its integration into a larger-scale industrial or domestic RES-based installation. Therefore, the results obtained from the prototype smart microgrid are scalable for the higher-power system. The motivation for the work described lies in the employment of the result obtained to subsequently undertake the design of a digital twin of the experimental PEMEL.

The structure of the rest of the manuscript is as follows. Section 2 describes the working principle of the PEMEL, as well as the model employed and the operation of the simulation platform. Section 3 explains the operation of the smart microgrid where the experimental PEMEL is integrated, detailing the relationship between its elements. Section 4 illustrates the data acquisition process and presents the case study. Finally, the main conclusions derived from the research are outlined.

2 PEMEL AND SIMULATION PLATFORM

This section describes the principle of operation and structure of PEMEL. Furthermore, a brief introduction of the models selected for this work is provided, as well as the working principle of the simulation platform.

2.1 Working Principle and Structure of PEMEL

As indicated in the previous section, PEMEL are hydrogen generation equipment based on the electrochemical process of electrolysis. This process involves the separation of a compound into its fundamental components using an electric current and a reduction and oxidation reaction. The hydrogen obtained from this process is often denoted with a colour that indicates the nature of the target compound for electrolysis (Ajanovic et al., 2022). For example, grey, brown, or black hydrogen comes from the electrolysis of fossil fuels and results in the emission of carbon dioxide during the process. Furthermore, the designation green is attributed to hydrogen derived from RES and characterized by the absence of pollutant-emitting components.

In RES-powered microgrids, PEMEL are employed for hydrogen generation from water, resulting in the production of hydrogen and oxygen in a clean and eco-friendly process. The reactions taking place at the anode and cathode of the PEMEL are defined in Equation (1) and Equation (2), respectively:

$$2H^+ + 2e^- \rightarrow H_2 \quad (1)$$

$$H_2O \rightarrow 2H^+ + \frac{1}{2}O_2 + 2e^- \quad (2)$$

The electrolysis process resulting from both sub-reactions is illustrated in Equation (3):

$$H_2O \rightarrow H_2 + \frac{1}{2}O_2 \quad (3)$$

Concerning its structure, the PEMEL comprises a collection of cells responsible for executing the electrolysis process. These cells can be interconnected either in series to form a stack or in parallel.

2.2 Selected Models

In order to comprehend the PEMEL behavior, a comprehensive selection of three models existing in previous literature has been chosen and integrated within the simulation platform. The selected models encompass Equivalent Circuit Models (ECM) that rely on an electrical diagram, thus facilitating the depiction of the device's behavior through the establishment of interrelationships amongst electrical components, including resistors and power sources.

In (Atlam & Kolhe, 2011) an ECM model for a PEMEL is presented, starting with the description of the model for a single PEM cell. Such work describes the relationship among its key variables, with a particular emphasis on the effects associated with voltage variations due to changes in temperature or operating pressure. Additionally, a scalable model is proposed for the PEMEL voltage, taking into account the structure and number of cells that compose the electrolyzer.

In (Awasthi et al., 2011), the model for a PEMEL operating at high temperature and pressure conditions (90 °C and 70 bar) is described. This model investigates the internal aspects that influence the PEMEL's operation, including factors such as partial pressures of water and hydrogen for the determination of the PEMEL voltage.

In the study of (Guilbert & Vitale, 2019) a dynamic analysis of a three-cell PEMEL is performed, resulting in an ECM model. This research illustrates the relationship between key variables of the PEMEL, such as power consumption, input current, voltage, and efficiency. Furthermore, the dynamic response of the stack voltage to variations in the input current is demonstrated.

The selected models have been employed while preserving their configuration parameters. Thus, the aim is to comprehend the operation of each model in its original state, without introducing any alterations that may disrupt its behavior throughout the simulation process or the comparison of results with other models or the experimental PEMEL.

2.3 Simulation Platform

The selected models have been implemented in a simulation platform that enables the individualized study of the behaviour of each model, as well as a comparison of the obtained results within a single tool. The simulation platform has been implemented in MATLAB software. The following MATLAB features/tools have been employed for this purpose: Simulink, App Designer, and the MATLAB workspace. The operational principle of the platform is founded on the interactions and synergies among these tools.

Simulink is an environment dedicated to the design and simulation of models and systems. This tool has been utilized to implement the selected models and to execute the simulations. App Designer, on the other hand, is a MATLAB toolbox specifically designed for the development of Graphical User Interfaces (GUI). This toolbox has been employed to create a GUI that serves as a control interface for the simulator and as a platform for the visualization of the simulations. Finally, the MATLAB workspace has been used as a connection bridge between the other environments, facilitating communication and data exchange. The diagram in Figure 1 illustrates the tools utilized in the operation of the simulation platform, as well as the diverse interactions among them.

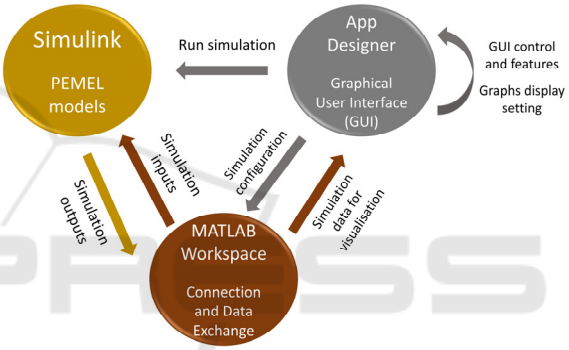

Figure 1: Simulation platform. Interactions between tools.

To facilitate the management of the simulation platform, users are provided with a GUI that operates based on navigation across various tabs. The GUI initiates by displaying a main tab, comprising buttons that grant access to the specific tabs of each model, as well as a tab dedicated to the comparison of model results. Furthermore, each model tab includes an additional tab devoted to the visualization of simulation results through graphical representations.

In (Gaspar et al., 2021), a detailed description of the operation, design and structure of the simulation platform employed in this work is provided, along with the integrated GUI and its implementation.

3 SMART MICROGRID AND EXPERIMENTAL PEMEL

Section 3 describes the Smart microgrid where the experimental PEMEL is framed, detailing the equipment involved and their interactions. Moreover,

the technical specifications of the experimental PEMEL used in this work are detailed, as well as the auxiliary equipment, hardware, software and communications employed for its correct operation.

3.1 Smart Microgrid

The experimental PEMEL under study in this work is integrated into a prototype smart microgrid powered by RES and hybridized with hydrogen. The smart microgrid consists of two systems. Firstly, there is the main generation and storage system, composed of a set of photovoltaic (PV) panels and a Lithium-Ion (Li-Ion) battery.

The hydrogen-based support system comprises a generation system employing a PEMEL, a storage system by means of metal hydride tanks, and an electrical generation system based on a PEM Fuel Cell (PEMFC). The PEMEL and PEMFC are connected to DC/DC converters in order to adjust the voltage setpoints of these devices with the central DC bus, whose voltage level is managed by the battery.

Lastly, a programmable electronic load is available to simulate different load profiles, thus generation an energy demand within the system.

The diagram in Figure 2 illustrates the components of each system that constitute the smart microgrid, as well as the interaction between them.

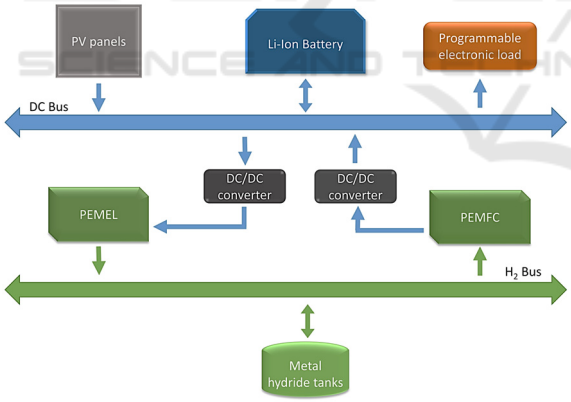

Figure 2: Component of the prototype smart microgrid.

The operation of the smart microgrid is as follows. The PV panels generate the required current to meet the energy demand imposed by the programmable electronic load. If there is an excess of electrical production beyond the energy demand, the remaining current is stored in the Li-Ion battery. If the State of Charge (SoC) of the battery exceeds an upper threshold, the surplus energy is transferred to the PEMEL for the generation of green hydrogen. This hydrogen is stored in the metal hydride tanks. In the event that the energy demand from the load exceeds the production from the PV panels, and the SoC of the battery is below a minimum threshold, the PEMFC is activated to generate electricity from the stored hydrogen. This ensures the required electrical current is supplied to the load.

3.2 Experimental PEMEL

The green hydrogen generation system consists of a six-cell PEM stack and a set of ancillary sensors and actuators that facilitate data acquisition and operational control of the PEMEL. Figure 3 illustrates the appearance of the experimental PEMEL, which has been equipped with a temperature sensor and a fan to regulate the working temperature. Table 1 provides the main technical specifications of the experimental PEMEL.

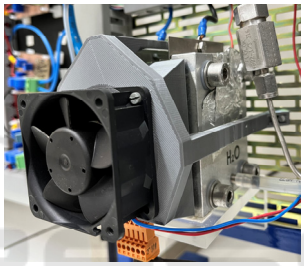

Figure 3: Experimental PEMEL appearance.

Table 1: Main technical specifications of the experimental PEMEL

Number of cells	6 cells in series
H_2 flow rate generated	250 ml/min; 15 l/h
H_2 purity	99.9999 %
Input current	Up to 8 A
Working temperature	25 to 50 ºC
Working pressure	Up to 6 bar

In Table 2, a series of measured variables and control signals for the operation of the PEMEL are listed, along with the components used for their measurement or actuation.

To centralize and manage data from the experimental PEMEL, a Programmable Logic Controller (PLC) is employed, which, in turn, sends this information to a dedicated SCADA system for real-time monitoring of the hydrogen generation system. The SCADA has been implemented using LabVIEW software, a specialized programming environment for designing such systems. The communication and data exchange between the PLC and SCADA have been resolved through the Open

Table 2: Measured variables and control signals for the operation of the PEMEL. Devices employed for measurement/actuation.

Measured variables / control signals	Devices
Voltage (V)	Potentiometer
Input current (A)	Hall effect sensor
Working temperature (ºC)	PT-100
Working pressure (bar)	Pressure sensor
Ambient temperature (ºC)	PT-100
Hydrogen flow rate (mL/min)	Thermal Mass Flow Meter
Water purge	Electrovalve
Feed water level	Electro-optical level sensor
ON/OFF power supply PEMEL	DC Relay

Platform Communications (OPC) protocol, specifically using its Data Access (DA) variant, which is widely used for data exchange in industrial environments (González et al., 2019). Additionally, the SCADA allows storing the visualized data in an Excel spreadsheet. The diagram in Figure 4 depicts the data flow from the PEMEL to its visualization in the SCADA, indicating the equipment, processes, and communication protocols involved.

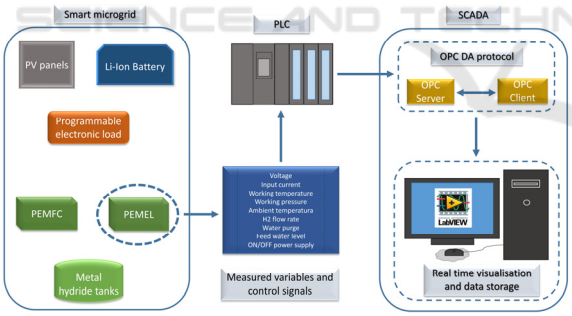

Figure 4: Flow data from PEMEL. Centralization, management and visualization.

4 RESULTS

This section details the results obtained from the application of the simulation platform. For this purpose, the conditions of the case study conducted are described, and a graphical comparative analysis of the behaviour of the models and the experimental PEMEL is conducted. Finally, conclusions are presented based on the results displayed.

4.1 Case Study

In order to perform a comparative analysis between the models and the experimental PEMEL, it is imperative to establish precise conditions for conducting the experimental tests. Subsequently, the measured experimental conditions will be replicated in the simulator to obtain results under comparable conditions. The conditions set for the experimental tests are as follows:

First, the experimental PEMEL starts from an idle state, performing an ascending path in the input current from 0 A to 8 A, with 0.2 A intervals and a settling time of 1 min.

Secondly, the experimental tests are conducted at atmospheric pressure (1 bar). This condition is imposed due to the technical limitations of the experimental PEMEL installation, which hampers a direct measurement of the pressures at the cathode and anode of the equipment. These pressures are required for the model of (Awasthi et al., 2011), so the PEMEL is operated at atmospheric pressure to maintain a fixed value for these variables. Furthermore, there is a specific interest in studying the isolated behavior of the experimental PEMEL, independent of any interaction with the other components of the installation. To achieve this, the PEM stack is disengaged from the storage system, facilitating the release of the generated hydrogen into the atmosphere.

The aim of this study is to acquire information from the measured variables in order to construct the characteristic curves that depict the behavior of the PEMEL.

4.2 Comparative Analysis

In order to perform the comparison of the obtained results, the characteristic curves of the models and the experimental PEMEL are grouped together and presented with a common legend. Firstly, the curves of the models are denoted by the name of the first author of the original research. For example, the model from (Atlam & Kolhe, 2011) is referred to as "Atlam." Additionally, a colour code is followed for each curve, using blue for Atlam, orange for Awasthi, grey for Guilbert, and yellow for the experimental PEMEL.

4.2.1 *I-V* Curve

The relationship between the input current (I) and the voltage of the PEMEL (V) forms the *I-V* characteristic curve, which is the main curve that describes the behavior of the equipment. This curve can be segmented into two operating regions. Initially, there is a current range spanning from 0 to 0.5 A, where the

voltage exhibits a significant increase, eventually stabilizing at an initial operating value. Subsequently, the *I-V* curve enters the nominal operating region, which extends from 0.5~1 A to 8 A. Within this region, the curve assumes a linear trajectory, with its slope varying based on the working temperature and pressure. Figure 5 illustrates the *I-V* curves for the various models as well as the experimental PEMEL.

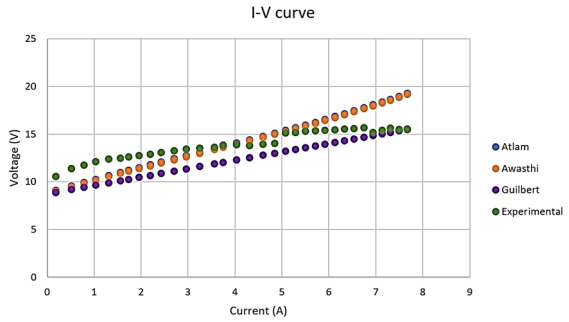

Figure 5: *I-V* curve.

In the mentioned figure, it can be observed that all curves follow the behavior described earlier. There is an initial current range with an initial operating voltage, followed by a linear operating range. For the model curves, the initial voltage starts around 9 V, followed by a distinct and pronounced increase.

The curves of Atlam and Awasthi exhibit similar values, tracing a parabolic trajectory where the voltage rises with the increase in input current, reaching a maximum of 19 V at 8 A. This trajectory is influenced by the increase in working temperature resulting from the operating time and input current consumed by the PEMEL.

The Guilbert curve follows a linear trajectory with a constant increment, reaching a maximum voltage of approximately 15 V. In this model, the voltage calculation is independent of the operating temperature, indicating that the voltage increase is solely due to the increase in input current.

On the other hand, the experimental curve shows a sudden increase in voltage, acquiring a higher value than the Atlam and Awasthi curves for low current ranges (0 to 2.5 A). In the nominal operating range, the I-V curve presents a lower slope than the curves of the models, resulting in approximate coincident values between 3 and 6 A. Finally, similar to the Guilbert model, the curve reaches a maximum value of approximately 15 V.

4.2.2 *I-P* Curve

The total consumed power (*P*) is directly proportional to *I* and *V*. This variable encompasses both the useful power employed by the PEMEL during the electrolysis process and the dissipated or lost power during the operation of the device. Figure 6 illustrates the *I-P* characteristic curve for the simulated models and the experimental PEMEL.

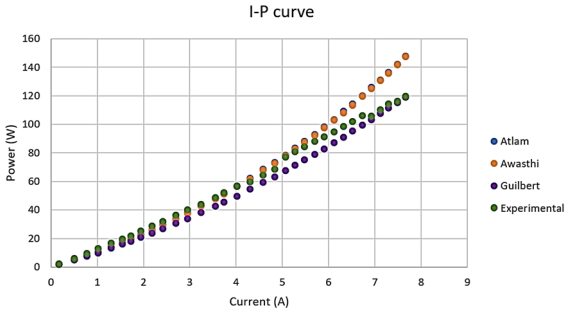

Figure 6: *I-P* curve.

In this figure, the direct relationship between *P* and *I* can be observed, where the value of *P* exhibits an increasing trend with increments in *I*. Furthermore, the trajectory and value of *P* in each curve are determined by the value of *V*. Similar to Figure 5, the maximum values of the curves are initially reached by the Atlam and Awasthi models. The minimum values of *P* are represented in the figure through the Guilbert curve. Finally, the *I-P* curve of the experimental PEMEL reflects intermediate values compared to those shown by the model curves.

4.2.3 *P-v*$_{H2}$ Curve

The hydrogen flow rate generated by the PEMEL (v_{H2}) is directly proportional to the consumed power. The *P*-v_{H2} characteristic curve, depicted in Figure 7, illustrates the relationship between the amount of product generated by the electrolyzer and the total energy consumption required.

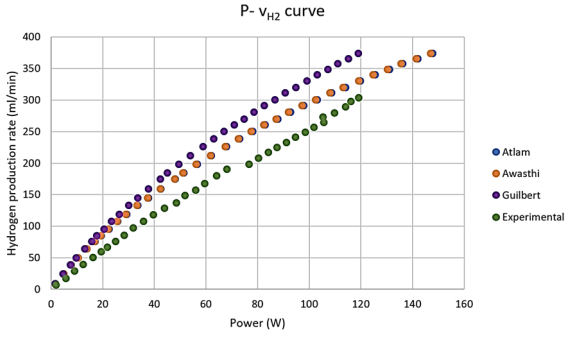

Figure 7: *P*-v_{H2} curve.

As observed in the figure, each curve exhibits a distinct trajectory. This occurrence is attributed to the

dependence of P on V, resulting in a relationship between the V-I and P-v_{H2} curves.

Regarding the models, the Guilbert, Atlam, and Awasthi curves exhibit a pronounced parabolic trajectory, with the Guilbert curve demonstrating the maximum v_{H2} values for a given current point. As for the experimental PEMEL, its curve follows a more linear path, reflecting the minimum values among the plotted curves. The figure illustrates how the nominal v_{H2} value (Table 1) is attained at a power value of 100 W.

4.2.4 *I*- η Curve

The efficiency of the PEMEL (η) is an indicator that reflects the overall operating performance of the equipment, encompassing all aspects that affect its operation. This parameter is determined by the ratio of the useful power employed in electrolysis and the total consumed power. Figure 8 depicts the I-η characteristic curve, illustrating the evolution of efficiency as a function of the input current.

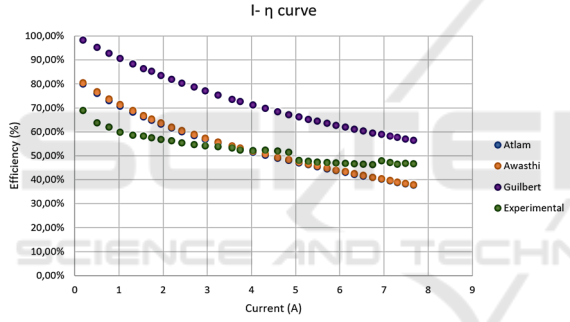

Figure 8: *I*- η curve.

In the figure, it can be observed that the efficiency of the experimental PEMEL remains around 50% within the nominal current range. On the other hand, the Guilbert curve estimates a maximum efficiency of around 60%, while the Atlam and Awasthi curves indicate an efficiency of approximately 40%.

The trajectory and form of these curves exhibit a reflection of the I-V curves depicted in Figure 5, owing to the dependence of η on P, and consequently on V. In fact, it can be observed that the experimental PEMEL curve and the curves of the Atlam and Awasthi models uphold similar values within the current range of 3 to 6 A, close to those presented in Figure 5.

4.3 Discussion

Following the results shown in the previous section, a series of conclusions can be drawn about the behaviour of the models and the experimental PEMEL.

Firstly, the characteristic curves that define the behaviour of the PEMEL are closely linked to the evolution of V during its operation. This fact reaffirms the importance of the I-V curve as the main characteristic curve of the device. The voltage level of the PEMEL conditions the total power consumed and, therefore, the hydrogen production and the efficiency of the equipment. Therefore, the trajectories of the I-P, P-v_{H2} and I-η curves are modified by the shape of the I-V curve.

Regarding the simulated models, the plotted characteristic curves illustrate a remarkable difference between the Guilbert model and the Atlam and Awasthi models. On the one hand, Atlam and Awasthi present curves with values close to each other due to their similar dependence on temperature and working pressure. However, a slight difference is observed in these curves, because the Awasthi model considers the partial pressures at the cathode and anode, as well as the variations in the ambient temperature surrounding the PEMEL. The Guilbert model, on the contrary, describes the behaviour of the PEMEL independently of the temperature and operating pressure of the equipment, which results in an I-V curve with a more linear trajectory and lower values with respect to V.

Common to all models, the values of v_{H2} shown in Figure 7 illustrate an over-estimation of hydrogen generation, reaching values much higher than those indicated in the technical specifications of the equipment. This leads to the future need to modify the models in order to adjust their behaviour to the technical limitations of the experimental PEMEL.

In relation to the experimental PEMEL, the behaviour of this device resembles those described by the Atlam and Awasthi models for nominal current range of 3 to 6 A. This range is contained within the operating current limits of the experimental PEMEL during the operation of the prototype smart microgrid.

Due to the above, and in order to design a model of the experimental PEMEL in the future, the Guilbert model is excluded and the Atlam and Awasthi models are chosen as possible base models.

5 CONCLUSIONS

This paper has presented the application of a simulation platform for the study of PEMEL models, along with an experimental comparison using a PEMEL integrated into a prototype smart microgrid hybridized with green hydrogen. The operational

principle of PEMEL has been described. Subsequently, the operation of the simulation platform has been illustrated, and the available models within it have been presented. Regarding the experimental PEMEL, its operation within the smart microgrid has been framed, including a description of the components comprising the microgrid and the installation implemented around the experimental PEMEL. The automation and supervision system applied to acquire and visualize experimental data has also been described. Finally, a case study has been illustrated through the comparison of characteristic curves of the PEMEL for the simulated models and the equipment in the microgrid.

In terms of future research aligned with this study, one potential avenue involves leveraging the simulation platform to adjust the characteristic parameters of the available models. The objective is to attain a model that accurately represents the behavior of the experimental PEMEL in order to develop a digital twin for the device. Another future endeavour entails utilizing the insights gained from comparing the obtained results. This knowledge can be applied to effectively integrate a PEMEL into larger-scale industrial or residential installations based on RES.

ACKNOWLEDGEMENTS

This project was supported by MCIN with funding from European Union NextGenerationEU (PRTR-C17.11) and by the Junta de Extremadura with funding from European Regional Development Funds (FEDER).

REFERENCES

Abdin, Z., Zafaranloo, A., Rafiee, A., Mérida, W., Lipiński, W., & Khalilpour, K. R. (2020). Hydrogen as an energy vector. *Renewable and Sustainable Energy Reviews*, *120*(November 2019).

Ajanovic, A., Sayer, M., & Haas, R. (2022). The economics and the environmental benignity of different colors of hydrogen. *International Journal of Hydrogen Energy*, *47*(57), 24136–24154.

Aminudin, M. A., Kamarudin, S. K., Lim, B. H., Majilan, E. H., Masdar, M. S., & Shaari, N. (2023). An overview: Current progress on hydrogen fuel cell vehicles. *International Journal of Hydrogen Energy*, *48*(11), 4371–4388.

Atlam, O., & Kolhe, M. (2011). Equivalent electrical model for a proton exchange membrane (PEM) electrolyser. *Energy Conversion and Management*, *52*(8–9), 2952–2957.

Awasthi, A., Scott, K., & Basu, S. (2011). Dynamic modeling and simulation of a proton exchange membrane electrolyzer for hydrogen production. *International Journal of Hydrogen Energy*, *36*(22), 14779–14786.

Falcão, D. S., & Pinto, A. M. F. R. (2020). A review on PEM electrolyzer modelling: Guidelines for beginners. In *Journal of Cleaner Production* (Vol. 261). Elsevier Ltd.

Feng, Q., Yuan, X. Z., Liu, G., Wei, B., Zhang, Z., Li, H., & Wang, H. (2017). A review of proton exchange membrane water electrolysis on degradation mechanisms and mitigation strategies. *Journal of Power Sources*, *366*, 33–55.

Folgado, F. J., González, I., & Calderón, A. J. (2022). Safety Measures for Hydrogen Generation Based on Sensor Signal Algorithms †. *Engineering Proceedings*, *27*(1).

Gaspar, F. J. F., Godoy, A. J. C., Pérez, I. G., Godoy, M. C., Calero, J. M. P., & Martín, D. O. (2021). Design of a simulation platform to test the suitability of different PEM electrolyzer models to implement digital replicas. *Proceedings of the 11th International Conference on Simulation and Modeling Methodologies, Technologies and Applications, SIMULTECH 2021*, 430–437.

González, I., Calderón, A. J., Figueiredo, J., & Sousa, J. M. C. (2019). A literature survey on open platform communications (OPC) applied to advanced industrial environments. *Electronics (Switzerland)*, *8*(5).

Guilbert, D., & Vitale, G. (2019). Dynamic emulation of a PEM electrolyzer by time constant based exponential model. *Energies*, *12*(4).

Ishaq, H., Dincer, I., & Crawford, C. (2022). A review on hydrogen production and utilization: Challenges and opportunities. *International Journal of Hydrogen Energy*, *47*(62), 26238–26264.

Ishaq, H., Siddiqui, O., Chehade, G., & Dincer, I. (2021). A solar and wind driven energy system for hydrogen and urea production with CO2 capturing. *International Journal of Hydrogen Energy*, *46*(6), 4749–4760.

Manna, J., Jha, P., Sarkhel, R., Banerjee, C., Tripathi, A. K., & Nouni, M. R. (2021). Opportunities for green hydrogen production in petroleum refining and ammonia synthesis industries in India. *International Journal of Hydrogen Energy*, *46*(77), 38212–38231.

Niermann, M., Beckendorff, A., Kaltschmitt, M., & Bonhoff, K. (2019). Liquid Organic Hydrogen Carrier (LOHC) – Assessment based on chemical and economic properties. *International Journal of Hydrogen Energy*, *44*(13), 6631–6654.

Potashnikov, V., Golub, A., Brody, M., & Lugovoy, O. (2022). Decarbonizing Russia: Leapfrogging from Fossil Fuel to Hydrogen. *Energies*, *15*(3).

Sarker, A. K., Azad, A. K., Rasul, M. G., & Doppalapudi, A. T. (2023). Prospect of Green Hydrogen Generation from Hybrid Renewable Energy Sources: A Review. *Energies*, *16*(3), 1–17.

Tang, D., Tan, G. L., Li, G. W., Liang, J. G., Ahmad, S. M., Bahadur, A., Humayun, M., Ullah, H., Khan, A., & Bououdina, M. (2023). State-of-the-art hydrogen generation techniques and storage methods: A critical review. *Journal of Energy Storage*, *64*(January), 107196.